Strain and relaxation effects in InAsP/InP multiple quantum well optical modulator devices grown by metal-organic vapor phase epitaxy

R. Y.-F. Yip,[a] A. Aït-Ouali, A. Bensaada, P. Desjardins,[b] M. Beaudoin,[c] L. Isnard,
J. L. Brebner, J. F. Currie, and R. A. Masut
Groupe de recherche en physique et technologie des couches minces (GCM), Département de génie physique, École Polytechnique de Montréal, et Département de physique, Université de Montréal, C.P. 6079, succ. ''Centre-Ville,'' Montréal QC, Canada H3C 3A7

(Received 26 August 1996; accepted for publication 7 November 1996)

Strained-layer multiple quantum well (MQW) InAsP/InP optical modulators have been fabricated from layers grown by metal-organic vapor phase epitaxy. The devices are a series of p-i(MQW)-n photodiodes in which the active core regions consist nominally of 25 periods of 10 nm InAsP quantum wells of 4.4%, 10.0%, 15.6%, and 26.4% As composition separated by 10 nm InP barriers. Structural parameters for the samples were obtained using high-resolution x-ray diffraction rocking curves and transmission electron microscopy. The series contains samples with both coherently strained and partially relaxed multi-layers where the relaxation is characterized by misfit dislocations. The band offsets for the heterostructures were determined by fitting the energy positions of the optical absorption peaks with those computed using the Marzin–Bastard model for strained-layer superlattices [as in M. Beaudoin *et al.*, Phys. Rev. B **53**, 1990 (1996)]. The conduction band discontinuities thus obtained are linear in the As composition (7.56 ± 0.08 meV per As % in the InAsP layer) at low and room temperature for As concentrations up to 39%, and up to 17% average relaxation. Comparisons between the coherently strained and partially relaxed samples demonstrated a broadening of optical transition linewidths due to relaxation which appears to be of minor consequence for optical modulator devices as the essential optical and electrical properties remain intact. The electric field-dependent red-shift of the $n=1$ electron-heavy hole transition was measured by a photocurrent method and found to be enhanced in structures with lower barrier heights. © *1997 American Institute of Physics.* [S0021-8979(97)02804-1]

I. INTRODUCTION

The growth of alloy semiconductor thin films to create the desired energy band structure for a device application often involves strained-layer epitaxy. In the case of III-V semiconductor lasers, the benefits of strain-induced modifications to the valence band structure of the material are widely recognized.[1–4] Device designs seek to maximize these benefits by introducing the largest possible strains without compromising the integrity of the crystal. However, it is difficult to avoid introducing at least some misfit dislocations into the device layers. In large lattice mismatch heteroepitaxy, misfit dislocation networks (MDNs) are deliberately introduced via buffer layers to relieve stress in the layers and control the relaxation process.[5–9] Dislocations resulting from relaxation are therefore present in many strained-layer devices and studying how they may affect overall device performance is of prime importance. For example, the dislocations in the active layers of semiconductor lasers are efficient non-radiative recombination centers and play a role in both rapid and gradual degradation processes.[10–13] In transistors and transport devices, dislocations act as effective scattering potentials and introduce deep trap states[14,15] with deleterious effects on the electronic mobility and high frequency operation. Very low defect densities in the active layers of these devices are usually catastrophic for both performance and reliability.

p-i-n photodiode devices appear not to be as seriously affected by the presence of moderate MDN densities in their layer structures. This is mostly due to two factors. First, relaxation and stress relief in strained systems can proceed principally via the formation of MDNs near the interfaces bordering a strained layer.[15,16] In this case, there can be few dislocations threading through the core section of the strain layer or superlattice forming the main light absorbing region of a photodiode and good optical absorption characteristics are preserved. Secondly, both the photonic and electrical power densities in these devices are usually very low so that little energy is available to perturb the defect states and drive further plastic relaxation of the crystal. Relaxed layers have previously been used to fabricate InAsP/InP multi-quantum well (MQW) p-i-n optical modulators[17,18] based on the quantum-confined Stark effect[19] (QCSE), where the InAsP grown on InP is compressively strained with a mismatch of up to 3.23%. The structural and optical properties of InAsP/InP multi-quantum well structures (MQWSs) have also been studied using high resolution x-ray diffraction (HRXRD) and transmission electron microscopy (TEM) to characterize both coherently-strained and relaxed structures[20,21] in which the Marzin–Bastard envelope function formalism[22] was used to fit the optical absorption transition peaks to the quantum well energy levels. These structural studies confirmed that

[a]Electronic mail: ryip@email:phys.polymtl.ca
[b]Present address: Coordinated Science Laboratory, University of Illinois at Urbana—Champaign, IL 61801.
[c]Present address: Advanced Materials and Process Engineering Laboratory, Department of Physics and Astronomy, University of British Columbia, Vancouver, BC, Canada V6T 1Z4.

Downloaded¬12¬Oct¬2007¬to¬132.204.76.245.¬Redistribution¬subject¬to¬AIP¬license¬or¬copyright,¬see¬http://jap.aip.org/jap/copyright.jsp

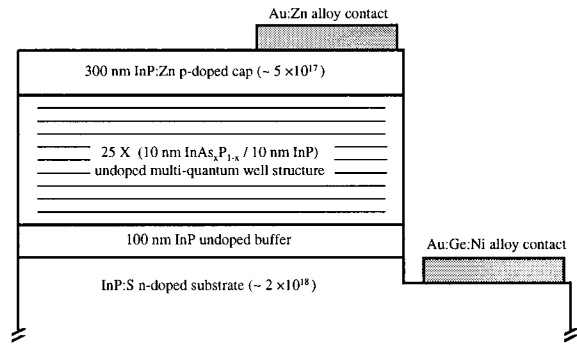

FIG. 1. Nominal layer and device structure for p-i(multi-quantum-well)-n optical modulators.

the relaxation in this system for moderate strains does indeed proceed via the generation of MDNs localized at the interfaces bordering the InAsP/InP MQWS. Thus, the MQW optical modulator in the InAsP/InP strained-layer system is a good candidate with which to study some of the effects of relaxation on device performance. In this paper, we present structural and optical characterizations of a series of InAsP/InP MQW layers and optical modulator devices which were fabricated with these layers. The As compositions and MQW layer thicknesses in the series were chosen to give samples with increasing degrees of relaxation. The operation of these devices appears not to be significantly affected by the presence of relaxation and we argue that the QCSE modulator may be an example of a device where strain relaxation and dislocations do not seriously affect the high frequency operation.

II. EXPERIMENT

The epitaxial layers for this study were prepared by low-pressure metal-organic vapor phase epitaxy (LP-MOVPE) using trimethyl-indium, tertiarybutyl arsine and phosphine precursors, and doped with diethylzinc and silane. The epilayer growth on S-doped ($\sim 2\times10^{18}$ cm^{-3}) InP (001) substrates was carried out using Pd-purified H_2 as a carrier gas and with a substrate temperature of 600 °C, a reactor pressure of 40 Torr, and a total gas flow rate of 2880 sccm.[23] We estimate that the flow velocity at the substrate under these conditions is 60 cm/s. The nominal layer and device structure for the samples is shown in Figure 1 and detailed in Table I. mod03, mod04, mod05, mod06, and mod07 were grown in a single series and the devices were fabricated in a single batch. mod07 is a control sample identical to the other samples in the series but with the MQWS replaced by a single uninterrupted section of undoped InP. mod02 was produced in a different run using the same growth parameters but differs from the others in the thicknesses and number of its constituent layers.[24] However, it has been extensively characterized by TEM, HRXRD and optical absorption and many of its structural characteristics have been precisely determined.[21] Thus, it serves as an important reference and is included in the current discussion.

Both symmetric (004) and asymmetric (115+/115−) HRXRD rocking curves for the samples were acquired using a Cu-Kα_1 x-ray source and a Philips four-crystal diffractometer with the monochromator aligned to Ge(220). TEM samples with $\langle 110\rangle$ surface normals were prepared by mechanical polishing followed by low-angle (4°) Ar^+ ion milling at 5 keV. The ion energy was gradually reduced to 2.5 keV during the final stages of thinning to reduce damage. The cross-sectional observations were made with a Philips CM30 microscope operated at 300 kV. Optical absorption spectra from 8 K up to room temperature were measured for the as-grown epitaxial layers using a free-flow, He-circulating cryostat with optical ports and a BOMEM DA3 Fourier transform interferometric spectrometer with a quartz halogen broad-spectrum source and Ge photodetector.

Following the material characterization steps, photolithographically defined circular device isolation mesas with diameters ranging from 100 μm to 800 μm were formed by etching through the epitaxial layers down to the substrate in a solution of $HCl:CH_3COOH:H_2O_2$.[25] Lift-off photolithography was used to pattern 200 nm thick layers of thermally evaporated Au-12% wt. Ge alloy metal onto the n-InP substrate and Au-10% wt. Zn alloy metal onto the p-doped cap. The samples were subjected to a single flash anneal cycle of 2 s at 300 °C to improve the contact resistivity.

In forward bias, turn-on voltages for the diodes ranged from 0.7 V to 1.0 V. Reverse-bias behavior varied from avalanche breakdown starting near −6 V up to Zener breakdown in excess of −15 V. Room temperature measurements of the electric field-induced Stark shift of the quantum well optical transitions were performed by detecting the photocur-

TABLE I. Sample listing and structural parameters obtained from high-resolution (115+/115−) and (004) XRD scans. Using mismatches measured with respect to InP, the fully relaxed, free-standing lattice parameter of the InAsP quantum well sections was deduced from a knowledge of the lattice parameters for the strain-distorted unit cell. This was subsequently used to compute the As composition of the wells, biaxial well strain and relaxation R). $h/hc_1$and h/hc_2 are the ratios, respectively excluding and including teh cap layer, of the multi-layer structure thickness to the Matthews–Blakeslee critical limit for a layer of the average composition.

	Multi-layer structure		Critical limit		In-plane mismatch		Biaxial strain in wells		R	
Sample	Multi-quantum well structure	Cap layer	h/hc_1	h/hc_2	[110]	$[1\bar{1}0]$	[110]	$[1\bar{1}0]$	[110]	$[1\bar{1}0]$
mod07	500 nm InP	300 nm	⋯	⋯	⋯	⋯	⋯	⋯	⋯	⋯
mod03	25×(9.4 nm $InAs_{0.044}P_{0.956}$/9.4 nm InP)	280 nm	4.1	4.0	<0.001%		−0.14%		<1%	
mod05	25×(9.8 nm $InAs_{0.100}P_{0.900}$/9.8 nm InP)	290 nm	11	10	<0.001%		−0.31		<1%	
mod06	25×(10.3 nm $InAs_{0.156}P_{0.844}$/10.3 nm	310 nm	20	17	0.012%	0.003%	−0.49%		5%	1%
mod04	25×(9.8 nm $InAs_{0.264}P_{0.736}$/9.8nm InP)	290 nm	36	32	0.079%	0.034%	−0.81%	−0.77%	20%	9%
mod02	50×(11.9 nm $InAs_{0.135}P_{0.865}$/11.9 nm	1550 nm	39	24	0.050%	0.024%	−0.41%	−0.38%	23%	11%

Downloaded¬12¬Oct¬2007¬to¬132.204.76.245.¬Redistribution¬subject¬to¬AIP¬license¬or¬copyright,¬see¬http://jap.aip.org/jap/copyright.jsp

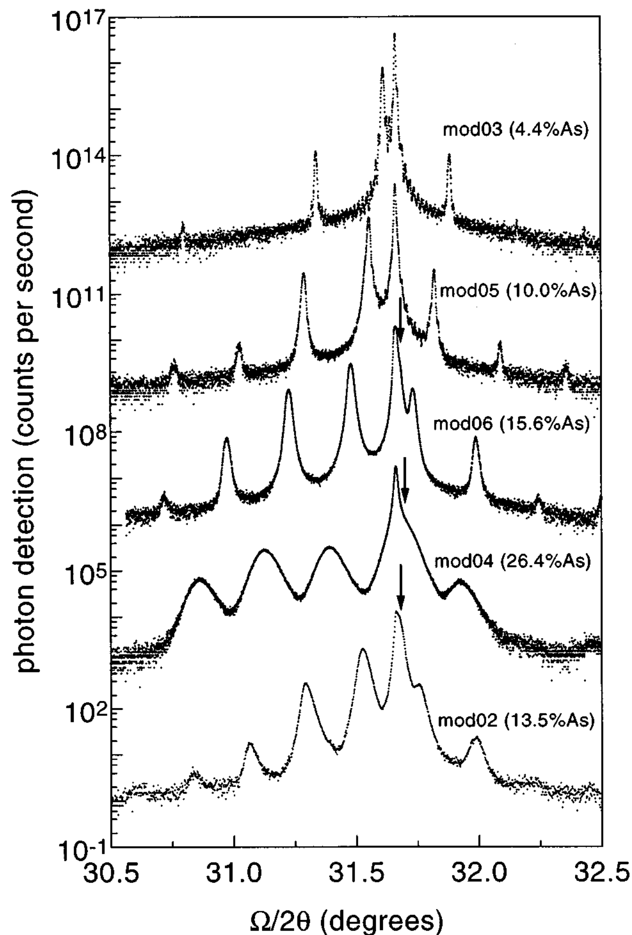

FIG. 2. Symmetric (004) reflection high-resolution x-ray diffraction rocking curves. The arrows indicate the approximate positions of separate peaks due to tensilely-strained InP material in the samples where plastic relaxation has been detected (see Table I).

rent response of the diodes as a function of reverse-bias voltage using a tungsten lamp source, 0.1 m scanning monochromator and lock-in amplifier. Temperature-dependent photocurrent spectra from 295 K down to 11 K were also measured for mod02, where the sample was attached to a copper cold-finger mount and placed in a closed-cycle, He-cooled cryostat with appropriate optical access ports.

III. RESULTS

A. Structural characterization

The HRXRD results are summarized in Table I and typical (004) rocking curves for the samples are displayed in Figure 2. The HRXRD data were analyzed with a combination of computer simulations of the rocking curves using dynamical diffraction theory[26] and some formal calculations. Details of the HRXRD analysis used can be found in Refs. 27–30. The three orthogonal components ([001], $[1\bar{1}0]$, and [110]) of the average MQWS mismatch with respect to InP, as defined by

$$\frac{\Delta a}{a} = \frac{a_{\mathrm{InAsP}} - a_{\mathrm{InP}}}{a_{\mathrm{InP}}} \tag{1}$$

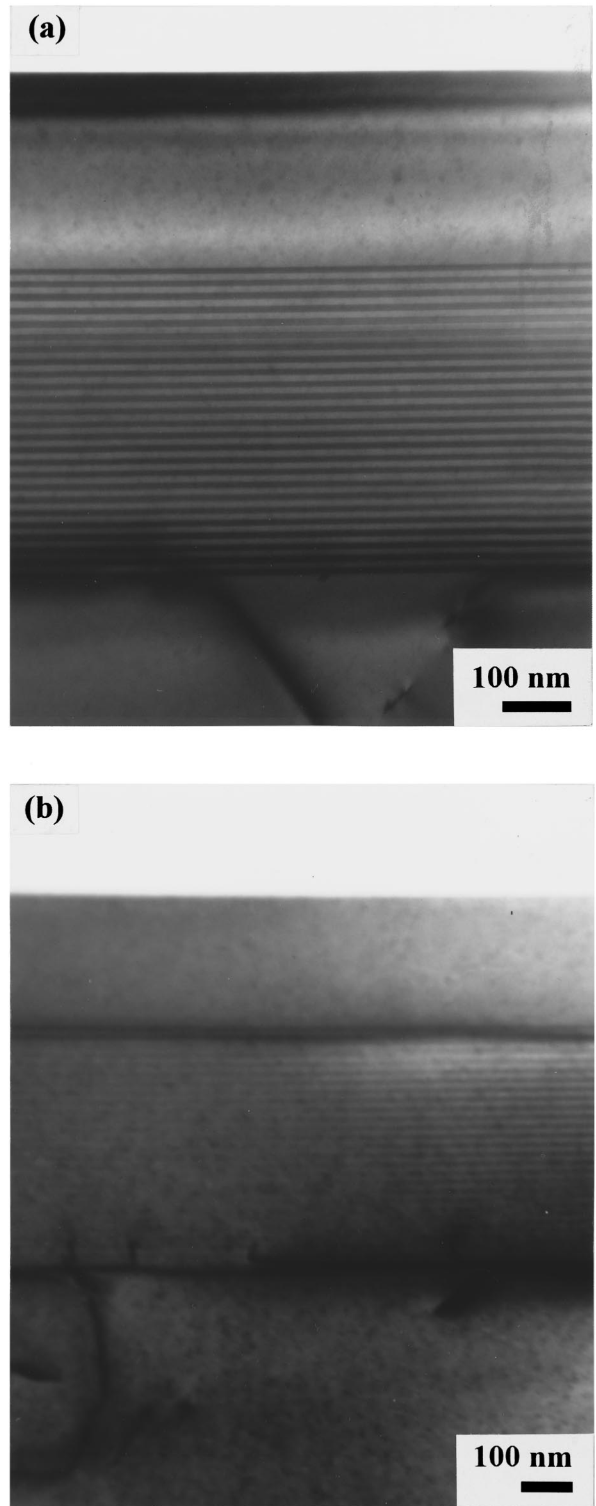

FIG. 3. Transmission electron microscopy bright-field images of mod04: (a) $g=(002)$, and (b) $g=(2\bar{2}0)$.

were determined from relative displacements of the zero order MQWS peaks with respect to the InP substrate peak in the HRXRD spectra. These mismatches gave the [001] $[1\bar{1}0]$, and [110] lattice constants for the strain-distorted unit cell; from which the lattice constant of the free-standing, fully relaxed unit cell, a_{free}, for the MQWS was recovered assuming a tetragonal distortion due to biaxial strain in the

Downloaded¬12¬Oct¬2007¬to¬132.204.76.245.¬Redistribution¬subject¬to¬AIP¬license¬or¬copyright,¬see¬http://jap.aip.org/jap/copyright.jsp

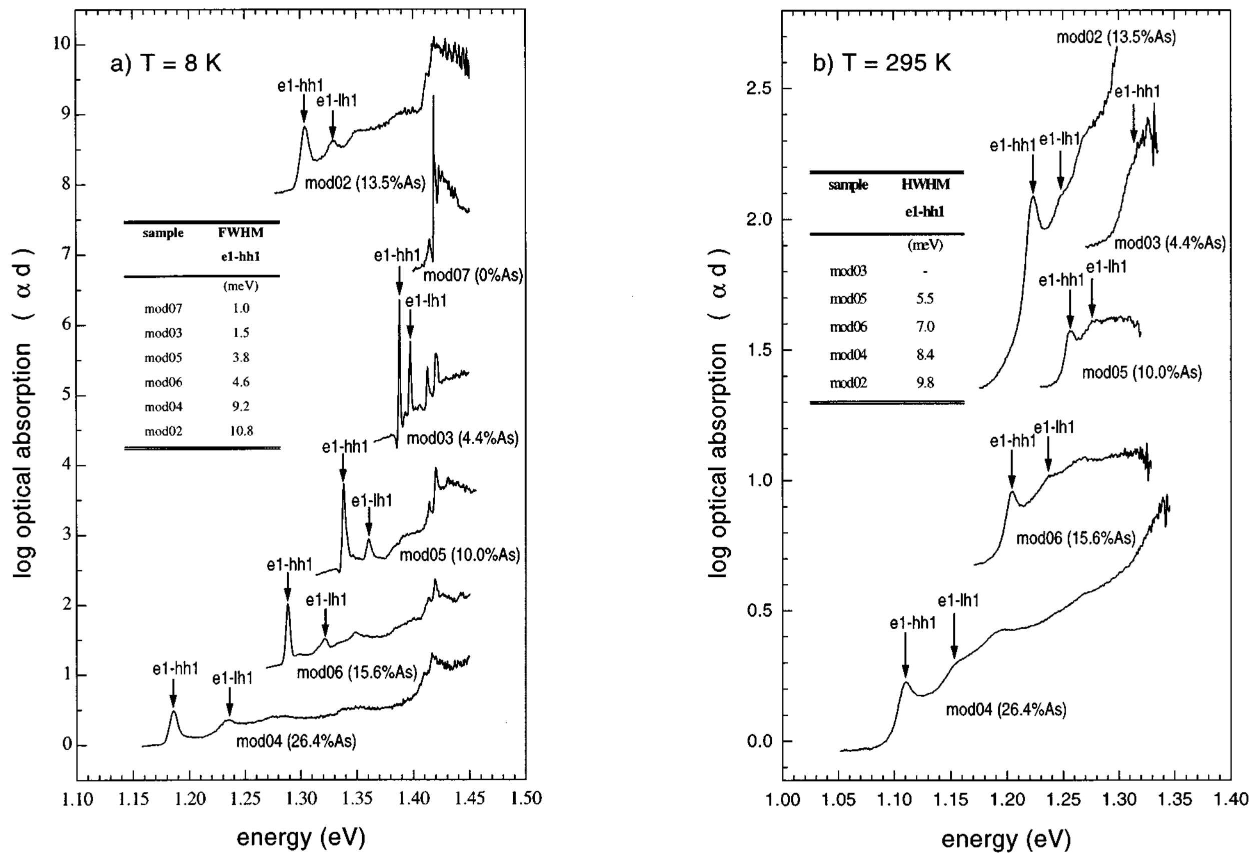

FIG. 4. Absolute optical absorption spectra for the as-grown epitaxial layers listed in Table I at (a) $T=8$ K and b) $T=295$ K. The $n=1$ electron-heavy hole (e1-hh1) and electron-light hole (e1-lh1) transitions are identified with arrows. The full width half maxima (FWHM) at $T=8$ K and half width half maxima (HWHM) at $T=295$ K for the e1-hh1 transitions are summarized in the inset tables.

(001) plane. The average As composition of the MQWS was then obtained from a_{free} by linear interpolation (Vegard's law) between the lattice constants of InAs and InP. Finally, from a knowledge of the lattice constants of the free-standing and distorted cubic cells, the biaxial strain in both wells and barriers was determined. For samples with plastic relaxation, the tensile strain in the barriers and cap layers is by definition the in-plane mismatch.

The ratios of the total MQWS thicknesses to their corresponding critical limits[31,32] for the formation of misfit dislocations has also been calculated and listed in Table 1 by considering the MQWS as single epitaxial layer of its average composition grown on a thick substrate. The relaxation, R, was computed using

$$R=\frac{a_{//}-a_{\mathrm{InP}}}{a_{free}-a_{\mathrm{InP}}} \tag{2}$$

where $a_{//}$ is one of the in-plane lattice constants.

We did not detect any relaxation in mod03 (1.9 hc) and mod05 (5.2 hc) and consider them to be coherently strained. However, the critical limits for the generation of misfit dislocations in equilibrium structures have been exceeded so that these are metastable structures and a very low density of misfit dislocations is possibly present in the two samples. mod06 (9.3 hc) is slightly-relaxed and likely has a low density MDN at the MQWS/buffer interface. mod04 (17 hc) and mod02 (18 hc) show very clear evidence of plastic relaxation. The TEM micrographs for mod04 (shown in Figure 3) and mod02 (shown in Ref. 21) confirmed the presence of MDNs at the MQWS/buffer and MQWS/cap interfaces. The relaxation is anisotropic (see Table I) and has been proceeded first via the generation of misfit dislocation lines parallel to $[1\bar{1}0]$ followed eventually by the same process to relieve stress along $[1\bar{1}0]$.[33]

The relaxation can also be observed qualitatively in the evolution of the symmetric (004) rocking curves of Figure 2. The spectra for mod03 and mod05 show sharp, intense peaks with the presence of finite thickness fringes, indicative of good layer perfection. The loss of such thickness fringes would be a good first indication of the presence of misfit dislocations.[30] The diffraction peaks for mod06 have a form similar to those of the coherently strained samples but the thickness fringes have disappeared and a slight broadening is detectable indicating that significant numbers of defects are just beginning to be introduced into the crystal at this strain energy. Dislocations distort the diffracting Bragg planes and cause broadening of the diffraction peaks.[28] The broadening that increases in the mod04 and mod02 peaks is due to their higher MDN densities. A small shoulder to the right of the substrate peak, indicated by the arrows, is perceptible in the spectra of mod06, mod04 and mod02. This corresponds to the signal from the InP material in the barriers and cap layer

Downloaded¬12¬Oct¬2007¬to¬132.204.76.245.¬Redistribution¬subject¬to¬AIP¬license¬or¬copyright,¬see¬http://jap.aip.org/jap/copyright.jsp

that is in tensile strain as a result of the plastic relaxation. These peaks shift to the right with increasing tensile strain as the in-plane mismatch increases. Note that the first order satellite peak of the MQWS in the mod04 spectrum is predicted to be nearly coincident with the substrate signal (the geometric mean of the zeroeth order and second order peaks). This indicates that the feature to the right of the substrate is largely due to the tensile-strained barriers and cap layer. In mod02, the shoulder remains closer to the substrate signal than in mod04 because the relaxation of the cap layer away from the MQWS is greater. The resolution in Figure 2 does not allow a precise determination but HRXRD scans using the diffractometer in its triple-axis mode with an additional 2-crystal analyzer at the detector confirmed the presence of separate substrate and tensilely strained InP peaks. The triple-axis measurements and TEM micrographs also showed that the MQWS/cap relaxation is more severe in mod02 than in mod04.

B. Optical absorption

The optical absorption spectra at 8 K and 295 K are displayed in Figure 4. These spectra are well-complemented by photoluminescence measurements that have also been performed on these samples and will be presented elsewhere.[34] Here, we focus the discussion exclusively on the behavior of the $n=1$ electron-heavy hole (e1-hh1) and electron-light hole (e1-lh1) band-edge transitions. The excitonic features associated with these optical transitions are identified with arrows and the absorption curves are displayed in the dimensionless units of the absorption coefficient, $\boldsymbol{\alpha}$, times the interaction length, **d**. For reference, the absorption coefficient due to the e1-hh1 transition in sample mod04, after normalizing to the total width of quantum well material, is $\sim 24000\ \mathrm{cm}^{-1}$ at 8 K and $\sim 11000\ \mathrm{cm}^{-1}$ at 295 K. Higher order transitions, such as those associated with the $n=2$ levels, are visible in most of the spectra and excitons associated with the InP band edge (~ 1.424 eV) are also well-resolved at 8 K. Notice that these latter excitons are slightly red-shifted in the mod06 (15.6% As) and mod04 (26.4% As) spectra due to the relaxation-induced tensile strain in the InP barrier and cap sections. There is significant relaxation in mod02 as well but the red-shifting is less evident because mod02 contains a much thicker InP buffer that is coherent with the substrate, and a thick cap that has relaxed away from the MQWS. mod02 (13.5% As) also contains ~ 2.4 times more quantum well material than the other samples. Hence, the sharper appearance of the mod02 absorption features relative to the other samples at 295 K is mostly a scaling effect.

In mod03 (4.4% As), the $n=1$ electronic level is only ~ 18 meV below the barrier level, and therefore less than the thermal energy at 295 K. Despite this, we had expected an excitonic feature to be clearly resolvable at 295 K because room-temperature excitonic features have been observed in shallow GaAs/AlGaAs MQWSs.[35] The lack of a clear excitonic feature at room-temperature for mod03 is due to the strain splitting of the hh1 and lh1 valence band levels. As a result, the mod03 absorption spectrum at 295 K comprises two broad excitonic features separated by only ~ 9 meV.

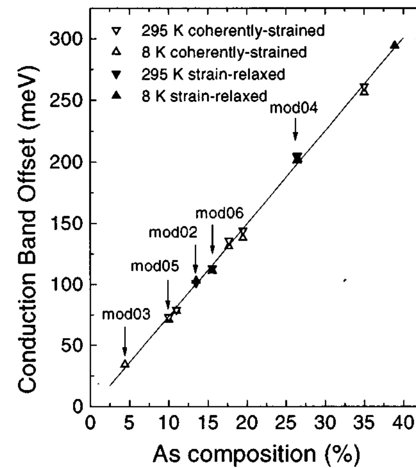

FIG. 5. Dependence of the absolute conduction band discontinuity, δE_C (meV), on the As composition, x, of the $InAs_xP_{1-x}$ quantum wells. The data points corresponding to samples in the current study are identified with arrows. The other points correspond to samples in Refs. 20 and 21. The linear least squares fit of the all the data points gives a slope of 7.56 ± 0.08 meV/As%.

Using the summary of absorption linewidths (see inset tables in Figure 4) as a guide to study the absorption spectra, we attribute the linewidth broadening trends to three main factors: temperature, alloy disordering, and relaxation. Temperature broadening effects add from 3.6 to 4.7 meV to the half widths and can be explained by LO phonon scattering of the excitons.[36,37] We attribute the broadening trend in the low temperature spectra for the samples without relaxation, mod07 (0% As), mod03 (4.4% As), and mod05 (10.0% As) to alloy disordering. This is an important effect as the linewidths increase rapidly with the As fraction. Unfortunately, it is difficult to discern clearly a broadening trend due to relaxation from that of alloy disorder in the subsequent samples mod06 (15.6% As), mod04 (26.4% As), and mod02 (13.5% As) because both increase with the As fraction.

A precise determination of the barrier heights and quantum well transition energy levels was made using the Marzin–Bastard envelope function model[22,38] and the structural and optical absorption data. Details of the calculation method and procedure can be found in Refs. 20–22. First, the structural parameters of the preceding section were used as inputs in the model considering the average value of the $[1\bar{1}0]$ and $[110]$ relaxation. From this, the model predicted the optical transitions for the samples for a given specification of the heterostructure conduction band offset, δE_C. Next, the excitonic binding energies and red-shift due to the built-in field had to be accounted for independently. Accordingly, nominal windows of 9 ± 3 meV and 6 ± 3 meV (the reduced mass of the e1-hh1 system is ~ 1.5 times that of the e1-lh1 system) were assigned for the binding energies of the hh and lh excitons, respectively. The red-shift of the e1-hh1 and e1-lh1 transitions for mod03, mod05, mod06, and mod04 due to the built-in field of ~ 17 kV/cm was estimated to be ~ 1 meV (see next section). The red-shift in mod02 was negligible because its undoped section is ~ 3.2 times thicker than that of the other samples, giving a built-in field

Downloaded¬12¬Oct¬2007¬to¬132.204.76.245.¬Redistribution¬subject¬to¬AIP¬license¬or¬copyright,¬see¬http://jap.aip.org/jap/copyright.jsp

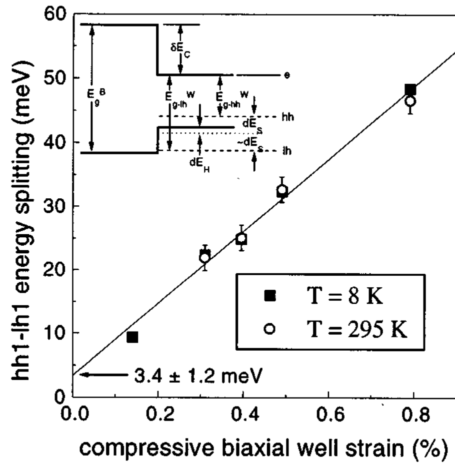

FIG. 6. Dependence of the $n=1$ electron-heavy hole (e1-hh1) and electron-light hole (e1-lh1) transition energy difference, as measured by optical absorption (Figure 3), on the compressive biaxial strain in the InAsP quantum wells, as measured by x-ray diffraction (Table I). The inset diagram (top left) illustrates the modification of the quantum well band gap due to compressive strain.

of only ~5 kV/cm. Finally, an optimal fit to the measured optical transitions was obtained by sweeping δE_C.

In Figure 5, the results for δE_C corresponding to the best fits are plotted against the As fraction in the InAsP quantum wells. All the points from Refs. 20 and 21 have been plotted along with those obtained in the current study. The plot of Figure 5 represents 20 band offset fits performed at 8 K and at room temperature on 11 InAsP/InP MQWSs. The 11 MQWSs span a range of As fractions from 4.4% to 38.9% of which 7 structures are coherently-strained and 4 structures have varying degrees of plastic relaxation. We observe that δE_C has a simple linear dependence on the As fraction (7.56 $\pm$0.08 meV/As%). In terms of the relative band offset, δE_C represents 75.8%$\pm$2.7% of the total strained band gap difference, δE_g. This linear dependence is consistent with the predictions of the quantum dipole model of Tersoff.[20,39]

An internal consistency check for the general accuracy of this analysis was performed. In Figure 6, the difference between the e1-lh1 and e1-hh1 optical transition energies, as measured by optical absorption, is plotted against the compressive biaxial strain in the InAsP quantum wells determined from the structural characterization by HRXRD. The inset in Figure 6 illustrates the strain-induced modifications to the well and barrier band gaps described by the strain Hamiltonian of Pikus and Bir.[40] Biaxial strain in the InAsP quantum wells introduces two general modifications to the band gap. First, the entire valence band structure is displaced relative to the conduction band by the hydrostatic deformation of the crystal. Then, the hh and lh bands are split by the shear deformation of the crystal. The case illustrated in the diagram is for coherent, compressive strain in the InAsP quantum wells. Any relaxation of the MQWS away from the substrate would introduce similar modifications to the InP barrier due to tensile strain. The influence of the strain anisotropy in the relaxed samples is negligible[21,41] and the average of the $[1\bar{1}0]$ and $[110]$ strains has been used. For small strains, the hh1-lh1 energy splitting induced by the shear term should have a nearly linear dependence on the biaxial well strain.[42] Therefore, we expect the hh1-lh1 energy difference to consist of a linear term due to the biaxial strain and an approximately constant term due to the binding energy difference between heavy and light hole excitons. The plot of Figure 6 affirms this and the linear least squares estimate for the intercept of 3.4$\pm$1.2 meV is in agreement with our previous assumptions about the exciton binding energies.

C. Quantum-confined Stark effect (QCSE)

The photocurrent responses of mod05 (10.0% As), mod06 (15.6% As), mod04 (26.4% As) at room temperature and of mod02 (13.5% As) at 11 K as a function of reverse-bias voltage are displayed in Figure 7. mod03 has not been included because thermal broadening makes it impossible to accurately determine the position of the e1-hh1 transition at room temperature. Using the photocurrent spectra and the

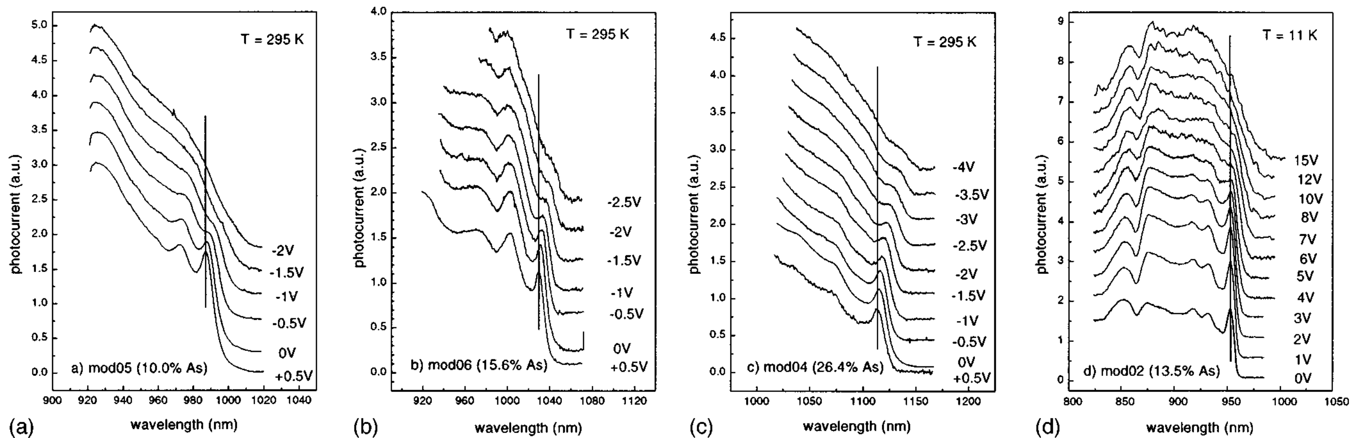

FIG. 7. Spectral photocurrent response of p-i(multi-quantum-well)-n diodes as a function of reverse-bias voltage at $T=295$ K for (a) mod05 (10.0% As), (b) mod06 (15.6% As), (c) mod04 (26.4% As) and at $T=11$ K for (d) mod02 (13.5% As). The nominal intrinsic layer thickness is 0.6 μm in (a), (b), (c), and 1.9 μm in (d).

Downloaded¬12¬Oct¬2007¬to¬132.204.76.245.¬Redistribution¬subject¬to¬AIP¬license¬or¬copyright,¬see¬http://jap.aip.org/jap/copyright.jsp

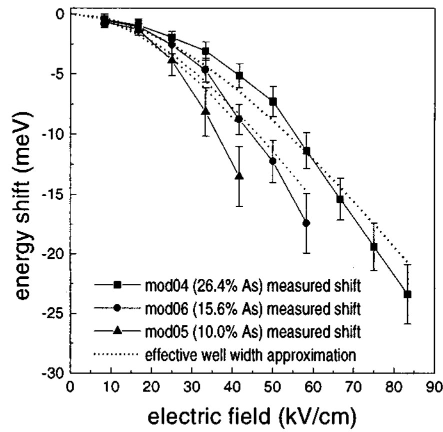

FIG. 8. The field-dependent energy red-shift of the quantum well levels for mod05 (10.0% As), mod06 (15.6% As), and mod04 (26.4% As) determined from the photocurrent curves (Figure 7). The shift as approximated by the effective well width method using the parameters in Table II is included for comparison.

optical absorption spectra, we estimated the electric field-induced red-shift of the e1-hh1 optical transition and the change in the optical absorption coefficient, $\Delta\alpha$. The analyses in the preceding sections provided an accurate knowledge of the quantum well widths, barrier heights, and energy levels for both conduction and valence bands. This allowed a calculation of the expected QCSE energy shift based on the ''effective well width'' method[19] (see Appendix). The measured and calculated energy shifts for mod05 (10.0% As), mod06 (15.6% As) and mod04 (26.4% As) are plotted in Figure 8 and the key parameters and results for the e1-hh1 transitions in these samples are summarized in Table II. The field dependence of the exciton binding energy is a comparatively small effect and has been neglected in the approximation.

$\Delta\alpha$ does not vary significantly among mod05 (10.0% As), mod06 (15.6% As), and mod04 (26.4% As) despite the differences in well depths, and degree of relaxation. The energy shifts in the relaxed samples are not detectably affected by the dislocations. The devices with shallower wells have less relaxation, less alloy disorder, and hence sharper zero-field excitons but also field ionize more easily. There is good agreement between measured curves and the effective well width approximation in the low to moderate field range. At higher fields, and especially for lower barrier heights, electron and hole wave functions penetrate significantly into the finite barriers and the approximation based on an infinite well loses validity. Under such conditions, the quasi-triangular barrier at the edge of the finite well is poorly approximated by the effective infinite well. Ultimately, all three devices give nearly the same change in absorption coefficient but this is achieved at significantly lower fields in the devices with shallower wells.

The behavior of mod02 is more difficult to analyze. In Figure 7(d), we display the photocurrent spectra acquired at 11 K because of its improved resolution. The usual field-induced broadening of the e1-hh1 and e1-lh1 excitonic levels is clearly apparent but *without* any appreciable red-shift. This is similar to simple field ionization of excitons by an electric field in the direction parallel to the quantum wells. However, the exciton peak remains well-resolved at an electric field of ~42 kV/cm (~8 V), a value well beyond the unconfined ionization field. The exciton broadens as if it were quantum-confined. It is unlikely that this is due simply to the presence of dislocations because the relaxation characteristics of mod02 are quite similar to those of mod04. However, unlike mod04, mod02 contains much thicker buffer and spacer layers. The MQWS in mod02 is separated from the heavily doped contact layers on both sides by ~360 nm spacer layers of undoped InP. These spacer layers containing MDNs could affect the process of photo-carrier collection and partly explain the behavior. mod02 is currently under continued investigation.

IV. DISCUSSION

In every sample, the widths of the individual InAsP quantum wells are below the Matthews–Blakeslee critical limit while the thickness of the MQWS exceeds it. The relaxation is therefore characterized by the generation of MDNs at the outer interfaces of the MQWS. This causes a broadening of the optical absorption transitions. The dislocations perturb the crystalline energy band structure presumably in a manner similar to the way they distort the diffracting Bragg planes and broaden peaks in the HRXRD rocking curves. However, the number of defects in the core of the MQWSs are sufficiently low that no dislocations threading through the MQWS in cross-section TEM measurements have been observed for either of the two extreme cases, mod04 (17 hc) and mod02 (18 hc). Thus as expected, the absorption and photocurrent spectra show that the good op-

TABLE II. Parameters used in the effective well width calculation. The barrier heights and E1 energies were obtained from the Marzin–Bastard envelope function calculation of the quantum well energies. E1 is the energy of the first quantized level with respect to the bottom of the well. The effective masses in the direction of the electric field are not significantly affected by strain so the values listed are linear interpolations between InAs and InP. The effective well widths are ''equivalent'' infinite well widths chosen such that the zero-field E1 energies match. $\Delta\alpha$ is the measured field-induced absorption coefficient change in each structure and the voltage at which it is attained.

	Quantum well region		Barrier heights		E1 levels		Effective masses		Effective well widths		
Sample	Well width	As content	e1	hh1	e1	hh1	e1	hh1	e1	hh1	$\Delta\alpha$
	(nm)	(%)	(meV)	(meV)	(meV)	(meV)	(m_0)	(m_0)	(nm)	(nm)	(cm^{-1}) $\pm$ 200
mod05	9.8	10.0	73	25	20	3.5	0.0734	0.626	16.0	13.0	2800@−1.0 V
mod06	10.3	15.6	113	39	24	3.7	0.0703	0.613	15.1	12.9	3100@−1.5 V
mod04	9.8	26.4	204	52	32	4.3	0.0642	0.587	13.5	12.2	3200@−2.5 V

Downloaded¬12¬Oct¬2007¬to¬132.204.76.245.¬Redistribution¬subject¬to¬AIP¬license¬or¬copyright,¬see¬http://jap.aip.org/jap/copyright.jsp

Ætical absorption properties of the light-absorbing intrinsic sections has been preserved. This the first criterion that must be satisfied for the use of relaxed layers in photodiode devices.

The second criterion to be satisfied is the preservation of the essential electrical characteristics of the diodes in reverse bias. In-plane charge transport is seriously compromised by MDNs but the geometry of photodiodes is more forgiving. For example, it has been shown that MDNs in the InGaAs base region of AlGaAs/InGaAs/GaAs heterojunction bipolar transistors generally do not influence the dc electrical behavior.[14] The operation of a QCSE optical modulator depends on the generation of rapid changes in the electric field across the MQWS junction; which in turn, is determined by charge transport to the heavily doped contact layers and capacitance effects across the junction. Because this does not rely on the transport of charge across the junction and through the MDNs, the generation and high frequency modulation of electric fields in the MQWS junction will not be greatly influenced by MDNs. The exception is at high fields near avalanche breakdown where the small number of dislocations that thread through the MQWS junction could facilitate charge leakage and the breakdown process. However, QCSE modulators are typically operated well below breakdown fields.

A more important concern is the effect of MDNs on the electric field uniformity. Non-uniformities could create significant field components parallel to the quantum wells and cause premature field broadening. In all the relaxed samples except mod02, the MDNs have formed very close to the heavily doped contact layers. The electrical response on the part of dislocation loops that extend into the contact layers is overwhelmingly screened by the large quantities of mobile charge. Hence, only the parts of the MDNs present in the undoped regions may appreciably affect the electric field. Placing the contact layers near the MQWS limits the extent of these potentially troublesome sections by making them very thin. As a result, the QCSE measurements in mod05, mod06 and mod04 have demonstrated that the MDNs generally do not affect the electric field uniformity across the layers at the typical operating voltages.

We also need to consider that MDNs may affect the transport of photo-charge away from the junction. Optical absorption in QCSE modulators may saturate when the photo-charge cannot be efficiently cleared from the quantum wells in the core of the MQWS[43] but the junction can typically never be overwhelmed by photocharge densities large enough to saturate the electric field. In these devices, the gross removal of such photo-charge from the junction is essentially a dc process and hence largely unaffected by MDNs. It is important to remember, however, that while the dc characteristics of charge transport can be generally unaffected by moderate MDN densities, the high frequency characteristics are seriously compromised. This is a critical consideration if the photodiode is to serve as a high speed detector. In such a case, the effect of MDNs on the carrier mobility limits the frequency response of the diode. Noise and dark current characteristics are also compromised.[8] A good strategy for minimizing any undesirable effects in all cases is to bury the MDNs in the heavily doped contact layers.

Finally, we observe that the energy shift per unit electric field is clearly greater in the samples with shallower wells in agreement with similar results in the GaAs/AlGaAs[43] system. This is a result of the influence of the finite barrier height on the energy of the first quantized level with respect to the bottom of the well, E1. As an alternative to the usual $m^*F^2L^4$ dependence,[44] the shift can be shown to be dependent on $F^2L^2/E1$ (see Appendix); where m^* is the effective mass, F is the electric field, and L is the quantum well width. Thus for two MQW systems having the same e1-hh1 transition energy, the one with wider and/or shallower wells will have a smaller E1 and demonstrate a larger shift for the same electric field. The use of shallower wells may not improve the maximum absorption coefficient change because of increased field broadening[45,46] of the excitonic feature, but an optical modulator using shallower wells may achieve useful on/off contrast ratios at lower fields. This is an important consideration for high-speed applications with severe drive voltage limitations.[47]

The barrier height effect indicates that a clear advantage exists for structures with large conduction band offsets. There is considerable evidence that field-induced broadening of the excitonic transitions is determined by the electronic confinement. Compared to the valence band, the conduction band wave functions are less well-confined and field-assisted electronic tunneling probabilities can be significant at relatively low fields.[45,46,48] For two heterostructures differing only in their band offsets, the shift will be enhanced in the one with the smaller valence band discontinuity since the valence band term dominates. At the same time, the enhanced electronic confinement in this structure will also improve the resistance of the exciton to field ionization. In particular, it may be interesting to compare the performance of strain-relaxed InAsP/InGaAsP/InP, or even InAsP/InAsP/InP, MQW modulators with lattice-matched InGaAsP/InGaAsP/InP[49] and InGaAs/InGaAsP/InP[50] MQW modulators for high-speed, low drive voltage applications at 1.3 μm and 1.55 μm. We expect that broadening due to MDNs at the outer interfaces of the separate confinement heterostructures in properly designed strained-layer InAsP structures can be largely compensated by: a ''faster'' shift and greater resistance to optical saturation by hole pile-up[43,50,51] due to the smaller valence band offset, superior electronic confinement due to the larger conduction band offset, reduced alloy disorder broadening and simplified growth conditions.

V. CONCLUSIONS

Strained-layer InAsP/InP p-i(MQW)-n optical modulators have been fabricated by MOVPE using layers with varying degrees of strain and relaxation. The samples have been characterized and analyzed using complementary HRXRD, TEM and optical absorption methods. We demonstrate in agreement with Refs. 20 and 21 that, following a determination of the multi-layer structural parameters, the e1-hh1 and e1-lh1 optical transition energies for such strained-layer superlattices may be accurately reproduced using the Marzin–

Downloaded¬12¬Oct¬2007¬to¬132.204.76.245.¬Redistribution¬subject¬to¬AIP¬license¬or¬copyright,¬see¬http://jap.aip.org/jap/copyright.jsp

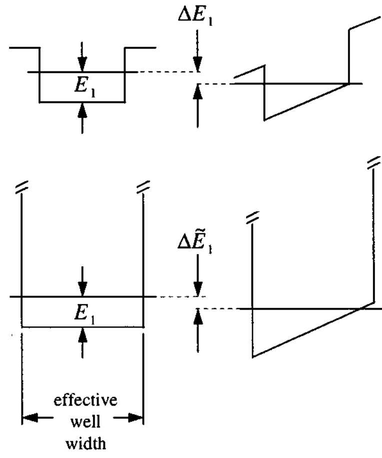

FIG. 9. The effective well width approximation.

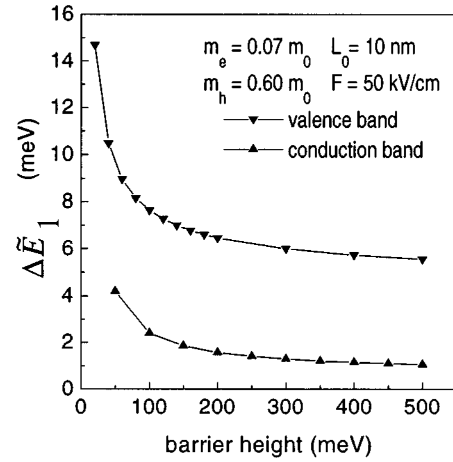

FIG. 10. The effect of variations in the finite barrier height on the QCSE calculated using the effective well width approximation for a typical InAsP/InP quantum well in the presence of a 50 kV/cm electric field.

Bastard model. Further evidence has been presented to support the hypothesis that the conduction band discontinuity for the InAsP/InP heterostructure follows a simple linear dependence on the As composition. Lower barrier heights in the MQWSs were found to enhance the QCSE red-shift and reduce the drive field. This latter result showed that QCSE optical modulator performance can be improved by using heterostructures with large conduction band offsets. Misfit dislocation networks resulting from plastic relaxation at the interfaces bordering the MQWSs broaden optical absorption linewidths and degrade modulator performance but the devices can continue to function quite acceptably. If such partially-relaxed structures can be stable, the use and control of misfit relaxation will in some instances allow a greater latitude in the design and fabrication of strained-layer materials and devices.

ACKNOWLEDGMENTS

We thank G. Turcotte and J. Bouchard for their excellent technical assistance in realizing this study. This work was supported by the Natural Sciences and Research Council (NSERC) of Canada and the Fonds pour la Formation de chercheurs et l'aide à la recherche (FCAR) du Québec.

APPENDIX: EFFECT OF FINITE BARRIER HEIGHT ON THE QUANTUM-CONFINED STARK EFFECT

An electric field applied perpendicular to a quantum well causes the discrete levels of the well to red-shift. However, the excitonic transitions associated with these levels can continue to be well-defined for fields that are many times the usual bulk ionization field because the conduction and valence band wave functions remain highly localized due to the quantum confinement. Thus according to Miller *et al.*,[19] large field-dependent changes in the band edge optical absorption are possible because the main excitonic transition at the band edge red-shifts appreciably before field broadening becomes severe.

The problem of electric field-dependent energy levels in a superlattice was first treated by Bastard *et al.*[44] using a variational method. The problem has since been studied by a variety of increasingly sophisticated methods.[19,45,46,48,52–54] The central issue in all formulations is that there do not exist any true bound states of the system for non-zero electric fields. Instead, we seek approximations to quasi-bound states that are long-lived. The usual strategy is to modify the band structure in the periphery of the quantum well to render the problem suitable for computation. Some recent approaches have given precise solutions for a wide variety of superlattice structures and electric field conditions.[45,46,48,54] However, these methods are complex and can obscure some of the fundamental physics. The original approach of Bastard *et al.*,[44] later extended by Miller *et al.*,[19] continues to be a very useful guide for designing optoelectronic devices because it provides an excellent insight into the physical situation. In this treatment of the problem, the response of the finite well to an applied electric field is approximated by the response of a wider infinite well, chosen so that their zero-field energy levels match (see Figure 9). An exact solution to the infinite well problem exists and the variational calculation of Ref. 44 gives an expression for the red-shift of the $n=1$ energy level, $\Delta\tilde{E}_1$, in the low-field limit as:

$$\Delta\tilde{E}_1 \cong -C_{\mathrm{var}}\frac{m^* e^2 F^2 L_{eff}^4}{\hbar^2} = -\frac{1}{8}\left(\frac{1}{3}-\frac{2}{\pi^2}\right)^2 \frac{m^* e^2 F^2 L_{eff}^4}{\hbar^2}; \quad \text{(A1)}$$

where m^* is the effective mass, e is the electronic charge, F is the electric field, and L_{eff} is the width of the effective infinite quantum well. This gives the well-known $\sim m^* F^2 L_{eff}^4$ dependence of the red-shift. Equation (A1) may be rewritten as:

$$\Delta\tilde{E}_1 \cong -\frac{1}{8}\left(\frac{1}{3}-\frac{2}{\pi^2}\right)^2 \frac{\pi^2}{2}\frac{e^2 F^2 L_{eff}^2}{E_1} = -C_{\mathrm{var}}\frac{\pi^2}{2}\frac{e^2 F^2 L_{eff}^2}{E_1} \quad \text{(A2)}$$

Downloaded¬12¬Oct¬2007¬to¬132.204.76.245.¬Redistribution¬subject¬to¬AIP¬license¬or¬copyright,¬see¬http://jap.aip.org/jap/copyright.jsp

with

$$E_1 = \frac{\hbar^2 \pi^2}{2m^* L_{eff}^2}. \tag{A3}$$

Hence, the red-shift varies as $\sim F^2 L_{eff}^2 / E_1$. In this paper, the solution to the zero-field finite well problem for E_1 has been given by an envelope function calculation using the Marzin–Bastard model, but a first approximation for multi-quantum well structures may be obtained by solving the usual relations for a single finite well:

$$E_1 = \frac{\hbar^2 \xi^2}{2m^* L_0^2} \tag{A4}$$

and

$$\xi^2 + \xi^2 \tan^2 \xi = \frac{2m^* L_0^2}{\hbar^2} V, \tag{A5}$$

where V is the barrier height. We make the distinction between the width of the finite well, L_0, and the width of the effective infinite well, L_{eff}. E_1 is the energy of the first quantized level with respect to the bottom of the *finite* well. Hence, the utility of (A2) is that it gives the dependence of the red-shift explicitly on E_1 and L_{eff}, which are functions of m^*, L_0, *and* the barrier height V.

Heuristically, energy levels close to the bottom of the well ''experience'' greater changes in the local energy structure following the application of an electric field and follow more closely the contours of the field-distorted quantum well. Consequently, the red-shift per unit field is larger for these levels. The asymptotic limit as E_1 tends to zero is $eFL_0/2$ by geometrical inspection. The dependence of $\Delta\widetilde{E}_1$ in (A2) on V for sample conditions in an InP-based quantum well is plotted in Figure 10. Most of the red-shift is developed in the valence band because it has a smaller E_1 due to the larger effective mass. Some caution should be exercised in interpreting the result as shallower wells giving larger shifts also suffer from enhanced field broadening. The present experiment with InAsP/InP quantum wells has shown that the excitonic features in the room temperature absorption spectra of quantum wells with electronic barriers of ~70 meV (mod05) are completely washed out by field broadening at only 30–40 kV/cm. Hence, efforts to reduce electronic barriers below this are dubious. Alternatively, Figure 10 shows that useful gains in $\Delta\widetilde{E}_1$, and hence ΔE_1, should be possible by diminishing the hole barriers into the sub-60 meV range. Whether or not using shallower and wider wells can enhance the maximal absorption coefficient change depends upon the particular MQW structure under consideration. However, genuine reductions in drive field should be possible in most cases.

[1] A. R. Adams, Electron. Lett. **22**, 249 (1986).
[2] E. Yablonovitch and E. O. Kane, J. Lightwave Technol. **6**, 1292 (1988).
[3] A. Kasukawa, T. Namegaya, T. Fukushima, N. Iwai, and T. Kikuta, IEEE J. Quantum Electron. **29**, 1528 (1993).
[4] M. Yamamoto, N. Yamamoto, and J. Nakano, IEEE J. Quantum Electron. **30**, 554 (1994).
[5] C. A. Tran, R. A. Masut, P. Cova, J. L. Brebner, and R. Leonelli, J. Cryst. Growth **121**, 365 (1992).
[6] R. Hull and J. C. Bean, in *Semiconductors and Semimetals* (Academic, San Diego, 1991), Vol. 33, p. 1.
[7] R. Beanland, D. J. Dunstan, and P. J. Goodhew, Adv. Phys. **45**, 87 (1996).
[8] K. R. Linga, G. H. Olsen, V. S. Ban, A. M. Joshi, and W. F. Kosonocky, J. Lightwave Technol. **10**, 1050 (1992).
[9] D. S. Kim, S. R. Forrest, G. H. Olsen, M. J. Lange, R. U. Martinelli, and N. J. Di Giuseppe, IEEE Photonics Technol. Lett. **7**, 911 (1995).
[10] S. N. G. Chu, S. Nakahara, M. E. Twigg, L. A. Koszi, E. J. Flynn, A. K. Chin, B. P. Segner, and W. D. Johnston, J. Appl. Phys. **63**, 611 (1988).
[11] B. C. de Cooman, C. W. T. Bulle-Lieuwma, J. A. de Poorter, and W. Nijman, J. Appl. Phys. **67**, 3919 (1990).
[12] P. G. Eliseev, *Reliability Problems of Semiconductor Lasers* (Nova Science, New York, 1991).
[13] S. N. G. Chu, MRS Bull, **43** (1993).
[14] Y. Ashizawa, S. Akbar, W. J. Schaff, L. F. Eastman. E. A. Fitzgerald, and D. G. Ast, J. Appl. Phys. **64**, 4065 (1988).
[15] Y. Uchida, H. Kakibayashi, and S. Goto, J. Appl. Phys. **74**, 6720 (1993).
[16] R. Hull, J. C. Bean, F. Cerdeira, A. T. Fiory, and J. M. Gibson, Appl. Phys. Lett. **48**, 56 (1986).
[17] T. K. Woodward, T. Sizer,II, and T. H. Chiu, Appl. Phys. Lett. **58**, 1366 (1991).
[18] T. K. Woodward, T. H. Chiu, and T. Sizer, II, Appl. Phys. Lett. **60**, 2846 (1992).
[19] D. A. B. Miller, D. S. Chemla, T. C. Damen, A. C. Gossard, W. Wiegmann, T. H. Wood, and C. A. Burrus, Phys. Rev. B **32**, 1043 (1985).
[20] M. Beaudoin, A. Bensaada, R. Leonelli, P. Desjardins, R. A. Masut, L. Isnard, A. Chennouf, and G. L'Espérance, Phys. Rev. B **53**, 1990 (1996).
[21] P. Desjardins, M. Beaudoin, R. Leonelli, G. L'Espérance, and R. A. Masut, J. Appl. Phys. **80**, 846 (1996).
[22] J. Y. Marzin, J. M. Gérard, P. Voisin, and J. A. Brum, in *Semiconductors and Semimetals* (Academic, San Diego, 1990), Vol. 32, p. 55.
[23] C. A. Tran, J. T. Graham, J. L. Brebner, and R. A. Masut, J. Electron. Mater. **23**, 1291 (1994).
[24] The epitaxial layers for mod02 consist of: 1200 nm p-doped cap, 360 nm undoped spacer, 50 periods of 11.9 nm InAsP/11.9 nm InP, 360 nm undoped spacer, and 1200 nm n-doped buffer layer grown on a S-doped ($\sim 2\times 10^{18}$cm^{-3}) InP(001) substrate.
[25] J. R. Flemish and K. A. Jones, J. Electrochem. Soc. **140**, 844 (1993).
[26] P. F. Fewster, Phillips J. Research **45**, 620 (1984).
[27] J. Hornstra and W. J. Bartels, J. Cryst. Growth **44**, 513 (1978).
[28] M. A. G. Halliwell, M. H. Lyons, S. T. Davey, M. Hockly, C. G. Tuppen, and C. J. Gibbings, Semicond. Sci. Technol. **4**, 10 (1989).
[29] P. F. Fewster, Semicond. Sci. Technol. **8**, 1915 (1993).
[30] M. A. G. Halliwell, Appl. Phys. A **58**, 135 (1994).
[31] The calculation has been performed assuming misfit dislocations of the 60° type and using the Fitzgerald formulation of the Matthews and Blakeslee model. See Refs. 7 and 32. The critical thicknesses obtained here differ from those in Ref. 21, where a smaller estimate for the in-plane component of the Burgers vector was used.
[32] J. W. Matthews and A. E. Blakeslee, J. Cryst. Growth **27**, 118 (1975); J. Cryst. Growth **29**, 273 (1975).
[33] K. L. Kavanagh, M. A. Capano, L. W. Hobbs, J. C. Barbour, P. M. J. Marée, W. Schaff, J. W. Mayer, D. Pettit, J. M. Woodall, J. A. Stroscio, and R. M. Feenstra, J. Appl. Phys. **64**, 4843 (1988).
[34] R. Y.-F. Yip *et al.* (unpublished).
[35] K. W. Goossen, J. E. Cunningham, and W. Y. Jan, Appl. Phys. Lett. **57**, 2582 (1990).
[36] J. Lee, E. S. Koteles, and M. O. Vassell, Phys. Rev. B **33**, 5512 (1986).
[37] M. Sugawara, T. Fujii, S. Yamazaki, and K. Nakajima, Phys. Rev. B **42**, 9587 (1990).
[38] G. Bastard, *Wave Mechanics Applied to Semiconductor Heterostructures* (les Éditions de Physique, Les Ulis Cedex, France, 1988).
[39] J. Tersoff, Phys. Rev. B **30**, 4874 (1984).
[40] G. E. Pikus and G. L. Bir, Sov. Phys. Solid State **1**, 136 (1959); *ibid.* **1**, 1502 (1960).
[41] A. Bensaada, A. Chennouf, R. W. Cochrane, J. T. Graham, R. Leonelli, and R. A. Masut, J. Appl. Phys. **75**, 3024 (1994).
[42] F.H. Pollak, in *Semiconductors and Semimetals* (Academic, San Diego, 1990), Vol. 32, p. 17.
[43] A. M. Fox, D. A. B. Miller, G. Livescu, J. E. Cunningham, and W. Y. Jan, IEEE J. Quantum Electron. **27**, 2281 (1991).
[44] G. Bastard, E. E. Mendez, L. L. Chang, and L. Esaki, Phys. Rev. B **28**, 3241 (1983).

Downloaded¬12¬Oct¬2007¬to¬132.204.76.245.¬Redistribution¬subject¬to¬AIP¬license¬or¬copyright,¬see¬http://jap.aip.org/jap/copyright.jsp

[45] T. Yamanaka, K. Wakita, and K. Yokoyama, Appl. Phys. Lett. **65**, 1540 (1994).
[46] T. Ikeda and H. Ishikawa, IEEE J. Quantum Electron. **32**, 284 (1996).
[47] I. Kotaka, K. Wakita, K. Kawano, M. Asai, and M. Naganuma, Electron. Lett. **27**, 2163 (1991).
[48] W. L. Bloss, J. Appl. Phys. **65**, 4789 (1989).
[49] H. Yamazaki, Y. Sakata, M. Yamaguchi, Y. Inomoto, and K. Komatsu, Electron. Lett. **32**, 109 (1996).
[50] M. Aoki, M. Suzuki, M. Takahashi, H. Sano, T. Ido, T. Kawano, and A. Takai, Electron. Lett. **28**, 1157 (1992).
[51] U. Koren, B. I. Miller, T. L. Koch, G. Eisenstein, R. S. Tucker, I. Bar-Joseph, and D. S. Chemla, Appl. Phys. Lett. **51**, 1132 (1987).
[52] E. J. Austin and M. Jaros, Phys. Rev. B **31**, 5569 (1985).
[53] J. Singh, Appl. Phys. Lett. **48**, 434 (1985).
[54] M.-E. Pistol and D. Gershoni, Phys. Rev. B **50**, 11738 (1994).

Downloaded¬12¬Oct¬2007¬to¬132.204.76.245.¬Redistribution¬subject¬to¬AIP¬license¬or¬copyright,¬see¬http://jap.aip.org/jap/copyright.jsp